

## STRUCTURE AND MAGNETIC PROPERTIES OF FINE $\text{Fe}_3\text{Mn}_3\text{O}_8$ FERRITE PARTICLES

Eva ŠVÁBENSKÁ<sup>1</sup>, Pavla ROUPCOVÁ<sup>1,2</sup>, Oldřich SCHNEEWEISS<sup>1</sup>

<sup>1</sup>*Institute of Physics of Materials, AS CR, Brno, Czech Republic, EU, [svabenska@jpm.cz](mailto:svabenska@jpm.cz)*

<sup>2</sup>*CEITEC Brno University of Technology, Brno, Czech Republic, EU*

<https://doi.org/10.37904/nanocon.2025.5207>

### Abstract

Manganese–iron  $\text{Fe}_3\text{Mn}_3\text{O}_8$  ferrite represents an important functional material for as catalytic purposes. In this study,  $\text{Fe}_3\text{Mn}_3\text{O}_8$  ferrite particles were synthesized and investigated with the aim of understanding its structure and magnetic behaviour. As a starting material, a manganese–iron precursor was prepared and its chemical composition verified by SEM/EDX, while X-ray diffraction (XRD) and Mössbauer spectroscopy provided insights into its crystal structure and local environment of iron. The precursor was subsequently annealed in a hydrogen atmosphere to obtain the final ferrite phase. The resulting Mn–Fe ferrite was analysed using the same structural and spectroscopic methods to confirm the transformation and purity of the product. In addition, its magnetic properties were investigated to obtain a comprehensive picture of its structural and magnetic characteristics.

**Keywords:** Manganese–iron ferrite, magnetic properties, Mössbauer spectroscopy, microscopy

### 1. INTRODUCTION

$\text{FeMnO}_x$  ferrites are highly promising materials among complex iron-manganese oxides, garnering significant interest for their dual functionality in both catalysis and magnetic applications [1]. Its performance as a catalyst is particularly evident in environmental and industrial processes, such as the low-temperature oxidation of volatile organic compounds like formaldehyde [2], ozonation catalysts [3], and the selective catalytic reduction (SCR) of nitrogen oxides ( $\text{NO}_x$ ) [4]. This high activity is attributed to the synergistic interaction between iron and manganese, as well as the material's excellent redox properties. Beyond its catalytic utility,  $\text{FeMnO}_x$  ferrites also exhibit valuable magnetic properties that enable practical solutions, including the easy magnetic separation and recovery of the catalyst after a reaction. The combination of these properties enhances its potential for developing highly efficient and reusable materials for a wide range of applications.

While most existing studies focus predominantly on catalytic performance or adsorption [2, 3, 4], the novelty of this work lies in its emphasis on the magnetic properties of  $\text{Fe}_3\text{Mn}_3\text{O}_8$ . The aim of this study is to provide a detailed investigation of the structural, spectroscopic, and especially the magnetic behaviour of the synthesized ferrite.

### 2. MATERIALS AND METHODS

#### 2.1 Sample preparation

Magnetic manganese ferrite was synthesized by thermal decomposition of a mixed Fe–Mn oxalate precursor in a hydrogen atmosphere at 400°C. The precursor, a mixed Fe–Mn oxalate, was obtained by precipitation from 0.1 M aqueous solutions of  $\text{FeSO}_4 \cdot 7\text{H}_2\text{O}$  and  $\text{MnSO}_4 \cdot \text{H}_2\text{O}$  with a 0.2 M solution of oxalic acid. The method of preparation of the oxalate precursor was similar to that in our previous study [5]. Both the precursor and the resulting manganese ferrite were characterised by electron microscopy, powder X-ray diffraction, and Mössbauer spectroscopy.

## 2.2 Experimental methods

The size and morphology of the synthesized specimens were characterized using scanning electron microscopy (SEM). SEM images were captured with a TESCAN LYRA 3XMU FEG/SEM equipped with an XMax80 Oxford Instruments detector for energy-dispersive X-ray analysis (EDS).

Phase composition studies were conducted using an Empyrean diffractometer from Panalytical in Bragg-Brentano geometry with  $\text{CoK}\alpha$  radiation ( $\lambda = 0.17902$  nm) at room temperature. The resulting patterns were analyzed using the HighScore® software and the ICDD database.

Magnetic properties, such as magnetic hysteresis loops and their parameters, were measured using a vibrating sample magnetometer (VSM) and an EverCool II Physical Property Measurement System (PPMS) from Quantum Design, in VSM mode, over a temperature range of 4-300 K and with a magnetic field range of  $\pm 9$  T.

The phase composition and magnetic state of the samples were analyzed using a standard Mössbauer spectrometer with a  $^{57}\text{Co}$  (Rh) radioactive source in transmission mode, covering the temperature range of 5–293 K. The computer processing of the spectra was done using CONFIT program package [6].

## 3. RESULTS AND DISCUSSION

### 3.1 Characterization of magnetic manganese ferrite

The morphology and elemental distribution of the manganese ferrite sample were examined by SEM/EDS. The results confirmed a homogeneous distribution of Fe and Mn (49.5 wt% Mn and 50.5 wt% Fe), indicating that the obtained material is not a simple physical mixture of two oxides. The particles exhibit predominantly rectangular to cubic shapes, often forming clusters of smaller crystallites, with particle sizes ranging from 0.7 to 4  $\mu\text{m}$ .

Phase composition was determined by powder X-ray diffraction (XRD). The diffraction pattern showed reflections at  $2\theta = 34.8^\circ, 41.0^\circ, 49.9^\circ, 62.2^\circ, 66.5^\circ, 73.3^\circ,$  and  $87.54^\circ$ , which match well with  $\text{Fe}_3\text{Mn}_3\text{O}_8$  (ICDD Ref. Code 98-002-8665) and correspond with results published by Xie [2] and France [4]. The average crystallite size, calculated from peak broadening, was 120.7 Å.

### 3.2 Magnetic measurements

The magnetic properties of our samples were investigated using a VSM and PPMS systems. Magnetic moments of the sample were measured as a function of temperature in the range 5-390 K and as a function of external magnetic field up to 30,000 Oe.

For the single-crystalline  $\text{FeMn}_2\text{O}_4$  sample, it was reported that it undergoes one structural and two magnetic transitions [7]. The structural transition occurs at  $T_s \sim 595$  K from cubic at high temperatures to tetragonal at low temperatures. Two magnetic transitions are ferrimagnetic at  $T_{\text{ferri1}} \sim 373$  K and  $T_{\text{ferri2}} \sim 50$  K, respectively.

Our results are summarised in **Figures 1-3**. The temperature dependences of magnetic moment in low field (remanent field of the superconducting magnet  $\sim 0.5$  Oe) drawn in **Figure 2a and 2b** show the presence of  $T_{\text{ferri1}}$  at  $\sim 388$  K and  $T_{\text{ferri2}}$  at  $\sim 52$  K. These values are in good agreement with the data in [7].

ZFC-FC measurements were carried out in external fields of 100, 200, and 300 Oe. Examples are shown in **Figure 3**. The shifts in blocking temperature  $T_B$  and irreversible temperature  $T_{\text{irr}}$  were observed after measurement in 200 and 300 Oe.

In the case of field 200 Oe, the values were transition temperature  $T_v = 118$  K, blocking temperature  $T_B = 164$  K, and irreversibility temperature  $T_{\text{irr}} \sim 260$  K. For measurements in field 300 Oe, the temperatures should have taken the following values: blocking temperature  $T_B = 140$  K, and irreversibility temperature  $T_{\text{irr}} \sim 275$  K.

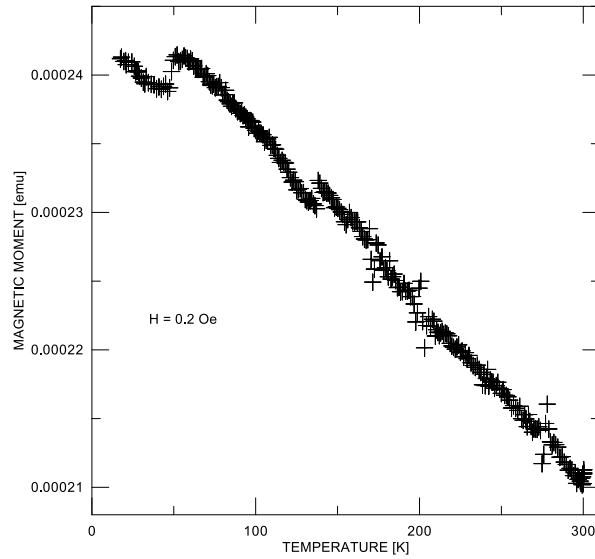


**Figure 1** Magnetic moment measured by cooling 300-5 K in magnet remanent field (~0.5 Oe).

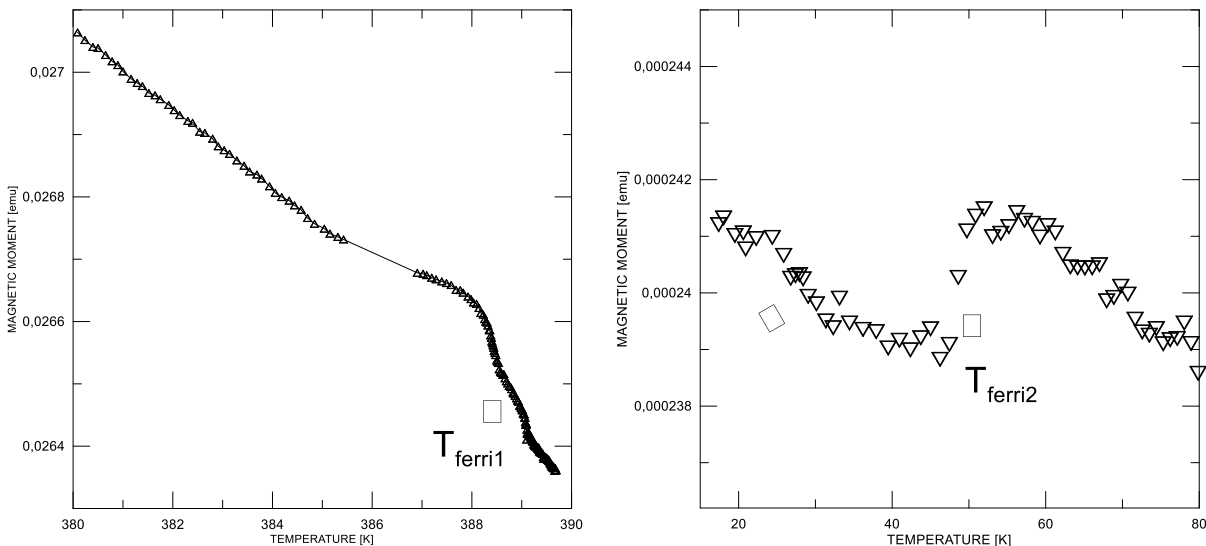


**Figure 2** Ferri1 and Ferri2 transformation temperatures detected in magnet remanent field (~0.5 Oe).

ZFC–FC measurements revealed that the blocking temperature decreases with increasing field, while the irreversibility temperature shifts to higher values, confirming strong field-dependent spin dynamics and complex magnetic transitions in  $\text{Fe}_3\text{Mn}_3\text{O}_8$ .

The hysteresis loops of  $\text{Fe}_3\text{Mn}_3\text{O}_8$  ferrite measured between 5 and 300 K confirm its soft ferrimagnetic character. The material exhibits a high magnetization at low temperatures, which decreases progressively with increasing temperature, reflecting thermal weakening of magnetic ordering. The loops are narrow with negligible coercivity, indicating low magnetic losses and easy magnetisation reversal. The parameters derived from the loops are summarised in **Table 1**. These results can be explained as a ferrimagnetic state below 300 K.

The hysteresis loop measured at 5 K after cooling in a field of 30000 Oe shows that exchange bias can be observed there. The parameters of the curves measured after cooling between 5 and 200 K are given in **Table 2**. The exchange bias and coercive force are increasing with decreasing temperature.

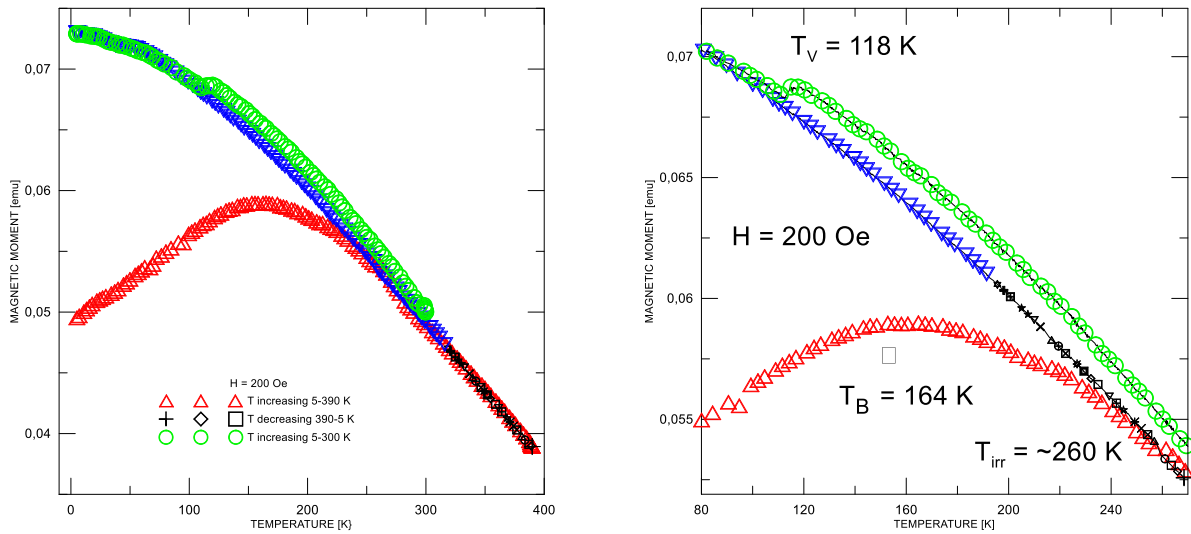


**Figure 3** Zero Field Cooling (ZFC) and Field Cooling (FC) curve in 200 Oe (left) and detailed ZFC-FC curve with marked  $T_B$  and  $T_V$  temperatures (right)

**Table 1** Parameters derived from the hysteresis loops ( $H_c$  coercive force,  $M_{max}$  moment at field 10000 Oe).

T [K]	$H_c$ [Oe]	$M_{max}$ [emu]
5	$650 \pm 5$	$0.175 \pm 0.015$
40	$425 \pm 5$	$0.170 \pm 0.015$
80	$270 \pm 5$	$0.165 \pm 0.015$
120	$180 \pm 5$	$0.155 \pm 0.015$
150	$140 \pm 5$	$0.150 \pm 0.015$
200	$80 \pm 5$	$0.142 \pm 0.015$
300	$45 \pm 5$	$0.108 \pm 0.015$
390	$0 \pm 5$	$0.079 \pm 0.015$

**Table 2** Parameters derived from the hysteresis loops after cooling in 30000 Oe ( $H_c$  coercive force,  $M_{max}$  moment at field 10000 Oe,  $H_e$  exchange bias shift).

T [K]	$H_c$ [Oe]	$M_{max}$ [emu]	$H_e$ [Oe]
5	$647 \pm 5$	$0.174 \pm 0.015$	$278 \pm 5$
40	$420 \pm 5$	$0.174 \pm 0.015$	$180 \pm 5$
80	$270 \pm 5$	$0.168 \pm 0.015$	$170 \pm 5$
120	$180 \pm 5$	$0.158 \pm 0.015$	$155 \pm 5$
150	$140 \pm 5$	$0.150 \pm 0.015$	$\sim 50 \pm 10$
200	$80 \pm 5$	$0.136 \pm 0.015$	$\sim 20 \pm 10$

### 3.3 Mössbauer spectroscopy

The examples of the  $^{57}\text{Fe}$  Mossbauer spectra and their analysis are shown in **Figure 4**. The parameters of the fitted components are summarised in **Table 3**. The clear difference between spectra taken at 300 K and 5 K can be explained as the result of the measuring time of an event on  $^{57}\text{Fe}$ , which is approximately  $10^{-7}$  seconds [8]. During this time interval, the iron atoms remain in a “stable” ferrimagnetic state.

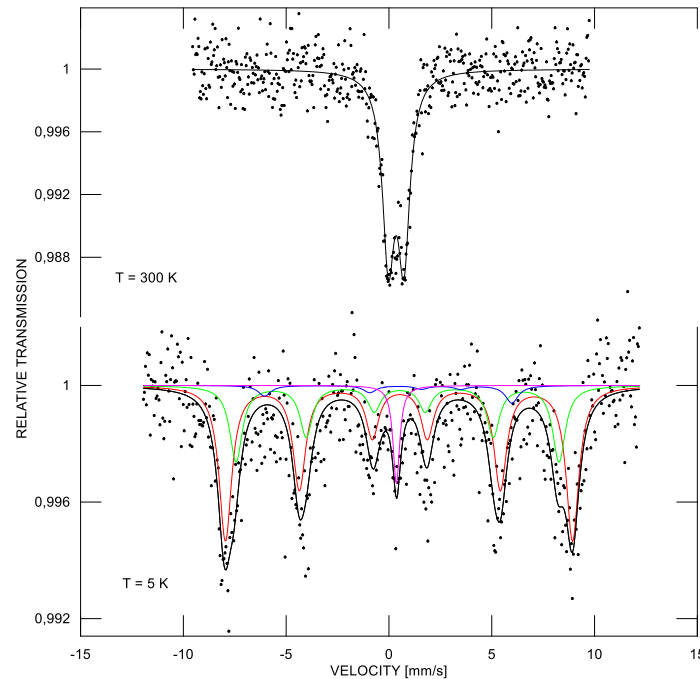


**Figure 4** Mössbauer spectra measured at 300 and 5 K. In the spectrum taken at 5 K, the fitted components are drawn.

**Table 3** Parameters of the fitted spectra (a component content in iron atomic fraction, IS isomer shift relative to  $\alpha$ -iron,  $Q_{\text{Spl}}/Q_{\text{Shift}}$  quadrupole splitting/quadrupole shift,  $B_{\text{hf}}$  hyperfine induction)

T [K]	component	a [a.f.]	IS [mm/s]	$Q_{\text{Spl}}/Q_{\text{Shift}}$ [mm/s]	$B_{\text{hf}}$ [T]
293	doublet	1.00	$0.34 \pm 0.02$	$0.75 \pm 0.02$	-
5	1 <sup>st</sup> sextet	$0.61 \pm 0.03$	$0.52 \pm 0.02$	$0.04 \pm 0.03$	$52.45 \pm 0.15$
	2 <sup>nd</sup> sextet	$0.30 \pm 0.03$	$0.47 \pm 0.03$	$0.11 \pm 0.06$	$48.80 \pm 0.29$
	3 <sup>rd</sup> sextet	$0.04 \pm 0.02$	$1.25 \pm 0.01$	$-2.59 \pm 0.01$	$37.29 \pm 0.02$
	singlet	$0.05 \pm 0.01$	$0.36 \pm 0.03$	-	-

#### 4. CONCLUSION

The present study demonstrates that  $\text{Fe}_3\text{Mn}_3\text{O}_8$  ferrite, synthesized through solid-state decomposition of an oxalate precursor, exhibits a combination of structural and magnetic features that extend its relevance beyond its commonly cited catalytic applications. While XRD and SEM/EDS confirm the formation of a fine-crystalline to nanocrystalline ferrite phase, the magnetic investigations reveal a much richer and previously underexplored behaviour. Two ferrimagnetic transitions, observed near 50 K and 388 K, indicate the presence of complex magnetic ordering that evolves over a broad temperature range. The pronounced dependence of ZFC–FC divergence on the applied field, along with the systematic decrease of both the blocking temperature  $T_B$  and irreversibility temperature  $T_{\text{irrev}}$  with increasing field, suggests field-tunable magnetic relaxation processes typically associated with nanoscale spin disorder or competing magnetic interactions. Furthermore, the emergence of exchange bias upon field cooling highlights interfacial magnetic coupling, which diminishes with temperature but remains significant within the studied range. Taken together, these findings reveal that  $\text{Fe}_3\text{Mn}_3\text{O}_8$  is not only structurally suitable for catalytic use but also possesses magnetic functionalities that may be exploitable in low-temperature spintronic, sensing, or magnetic storage systems.

## ACKNOWLEDGEMENTS

***This work has been created by financial support and using of the research infrastructure of the Institute of Physics of Materials Czech Academy of Sciences, v. v. i.; CzechNanoLab project LM2023051 funded by MEYS CR is gratefully acknowledged for the financial support of the measurements at CEITEC Nano Research Infrastructure.***

## REFERENCES

- [1] AKHLAGHI, N., NAJAFTOUR-DARZI, G. Manganese ferrite (MnFe<sub>2</sub>O<sub>4</sub>) Nanoparticles: From synthesis to application – A review. *Journal of Industrial and Engineering Chemistry*. 2021, Vol.103, pp. 292–304. Available from: <https://doi.org/10.1016/j.jiec.2021.07.043>
- [2] XIE, H., CHEN, X., ZHANG, Ch., LAO, Z., LIU, X., XIE, X., SEMIAT, R., ZHONG, Z. Identifying the Fe<sub>3</sub>Mn<sub>3</sub>O<sub>8</sub> phase as a superior catalyst for low-temperature catalytic oxidation of formaldehyde in air. *Environmental Science: Nano*. 2022, vol.9, Issue 2, pp. 767-780. Available from: <https://doi.org/10.1039/D1EN00923K>
- [3] DESAI, I., NADAGOUDA, M.N., ELOCITZ, M., MILLS, M., BOULANGER, B. Synthesis and characterization of magnetic manganese ferrites. *Materials Science for Energy Technologies*. 2019, Vol. 2, Issue 2, pp. 150-160. Available from: <https://doi.org/10.1016/j.mset.2019.01.009>
- [4] FRANCE, L.J., YANG, Q., Li, W., Chen, Z., Guang, J., GUO, D., WANG, L., Li, X. Ceria modified FeMnOx—Enhanced performance and sulphur resistance for low-temperature SCR of NOx. *Applied Catalysis B: Environmental*. 2017, Vol. 206, pp. 203–215. Available from: <https://doi.org/10.1016/j.apcatb.2017.01.019>
- [5] ŠVÁBENSKÁ, E., ROUPCOVÁ, P., HAVLÍČEK, L., SCHNEEWEISS, O. Mössbauer and magnetic studies on nanocrystalline FeNi particles prepared by thermal reduction. *Journal of Radioanalytical and Nuclear Chemistry*. 2025, Vol. 334, pp. 4171–4178. Available from: <https://doi.org/10.1007/s10967-024-09898-5>
- [6] ŽÁK, T., JIRÁSKOVÁ, Y. Confit: Mössbauer spectra fitting program. *Surface and Interface Analysis*. 2006, vol. 38, pp. 710–714. Available from: <https://doi.org/10.1002/sia.2285>
- [7] NEPAL, R., ZHANG, Q., DAI, S., TIAN, W., NAGLER, S.E., JIN, R., Structural and magnetic transitions in spinel FeMn<sub>2</sub>O<sub>4</sub> single crystals. *Physical Review B*. 2018, Vol. 97, pp. 024410. Available from: <https://doi.org/10.1103/PhysRevB.97.024410>
- [8] GONSER, U. Mössbauer Spectroscopy (Topics in Applied Physics, Vol. 5). Springer, Berlin, Heidelberg, New York, 1975.